JACS
JOURNAL OF THE AMERICAN CHEMICAL SOCIETY
pubs.acs.org/JACS
Article

Carbon Nano-onions: Potassium Intercalation and Reductive Covalent Functionalization

M. Eugenia Pérez-Ojeda,* Edison Castro, Claudia Kröckel, Matteo Andrea Lucherelli, Ursula Ludacka, Jani Kotakoski, Katharina Werbach, Herwig Peterlik, Manuel Melle-Franco, Julio C. Chacón-Torres, Frank Hauke, Luis Echegoyen,* Andreas Hirsch,* and Gonzalo Abellán*

Cite This: J. Am. Chem. Soc. 2021, 143, 18997−19007

ABSTRACT: Herein we report the synthesis of covalently functionalized carbon nano-onions (CNOs) via a reductive approach using unprecedented alkali-metal CNO intercalation compounds. For the first time, an *in situ* Raman study of the controlled intercalation process with potassium has been carried out revealing a Fano resonance in highly doped CNOs. The intercalation was further confirmed by electron energy loss spectroscopy and X-ray diffraction. Moreover, the experimental results have been rationalized with DFT calculations. Covalently functionalized CNO derivatives were synthesized by using phenyl iodide and *n*-hexyl iodide as electrophiles in model nucleophilic substitution reactions. The functionalized CNOs were exhaustively characterized by statistical Raman spectroscopy, thermogravimetric analysis coupled with gas chromatography and mass spectrometry, dynamic light scattering, UV−vis, and ATR-FTIR spectroscopies. This work provides important insights into the understanding of the basic principles of reductive CNOs functionalization and will pave the way for the use of CNOs in a wide range of potential applications, such as energy storage, photovoltaics, or molecular electronics.

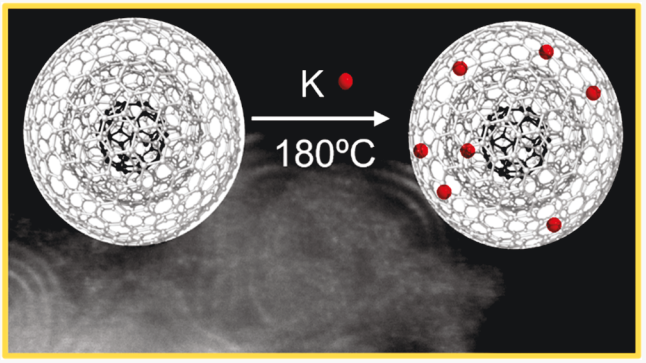

INTRODUCTION

Since the discovery of the fullerene C_{60} in 1985,[1] carbon nanomaterials have been investigated in different fields such as photovoltaics and biological applications.[2,3] In 1992, Ugarte[4] reported a new allotropic form of carbon known as carbon nano-onions (CNOs), which were first observed by Ijima in 1980.[5] These multishell fullerenes have received considerable attention during the past decade due to their outstanding properties such as a large surface area to volume ratio, low densities, and a graphitic multilayer morphology, which makes them excellent candidates for diverse applications, such as energy conversion and storage,[6] supercapacitors,[7] solid lubricants,[8,9] and cellular imaging and theranostics,[10,11] among others.[4,12−15]

CNOs can be synthesized through several methods, such as ball milling,[16] ion implantation,[17] arc discharge,[18] plasma treatment,[19] chemical vapor deposition,[20] laser ablation,[21] electron irradiation,[22] thermal decomposition of layered nanoreactors,[23,24] soft-chemistry methods,[25] and thermal annealing of detonation nanodiamonds (d-NDs) under either vacuum[26] or inert atmosphere.[27,28] The most common method for the synthesis of CNOs is based on the thermal annealing of d-NDs of about 5 nm diameter under a He atmosphere at temperatures between 1500 and 1800 °C.[29] Moreover, this method is highly reproducible and CNOs are obtained in quantitative yields, thus allowing a great potential for industrial applications.

Chemical functionalization has been extensively explored in order to modify the interfacial properties and modulate the solubility of CNOs, representing the most promising route for controlling their processability.[11,12,29,30] Their degree of functionalization is commonly associated with the size and strain of the CNOs. Typically, small-size CNOs (5−10 nm) are more reactive than larger-sized ones due to their higher curvature, leading to an increase in the pyramidalization of the C atoms.[28] Different synthetic procedures for CNO functionalization have been investigated using always neutral CNOs; however, the unambiguous characterization of the covalent functionalization in CNOs remains challenging. When it comes to other carbon allotropes, one of the probably most efficient routes for functionalization is the reduction using alkali metals

Received: July 21, 2021
Published: October 26, 2021

https://doi.org/10.1021/jacs.1c07604
J. Am. Chem. Soc. 2021, 143, 18997−19007

as performed in graphite intercalation compounds (GICs), followed by the quenching of the intermediately formed *graphenides*[2,31] with electrophiles.[3,32,33] Concerning the application of reductive approaches to CNOs, the number of examples is very scarce, with only one precedent employing a liquid Na−K alloy to activate the surface of the CNOs prior to the reaction with $C_{16}Br$.[30] It is important to highlight that CNOs exhibit great potential as electrode materials in energy storage devices in which thin-film processing and alkali-metal intercalation are key aspects; therefore, understanding these processes is a matter of utmost importance. Moreover, a controlled reductive functionalization would allow one to envision novel hybrid materials, including covalent intercarbon-allotrope architectures. However, the solid-state intercalation of CNOs with potassium and its ulterior functionalization with electrophiles remains completely unexplored.

Herein, we developed the vapor-phase intercalation of CNOs with alkali metals using high-vacuum conditions as well as a bulk solid-state reaction. For the first time, an *in situ* Raman study of the controlled intercalation process with potassium has been carried out in CNOs, revealing the development of a Fano resonance. Moreover, X-ray diffraction (XRD) and transmission electron microscopy (TEM) analysis allowed a direct observation of the change in the interlayer distance in CNOs after their intercalation and the localization of potassium atoms, respectively. Last but not least, we analyzed the functionalized CNOs by statistical Raman spectroscopy[34,35] (SRS) and thermogravimetric analysis coupled with gas-chromatographic separation and mass-spectrometric characterization (TGA/GC/MS), allowing a precise characterization, establishing clear spectroscopic fingerprints to understand the functionalization protocol in CNOs. This work provides a better insight of potassium intercalation in CNOs and the ulterior functionalization by different organic species.

RESULTS AND DISCUSSION

The first objective of our work is to investigate the effects of intercalation in CNOs by the intrusion of metallic potassium. The reductive approach via potassium intercalation has already been widely investigated on several carbon nanomaterials, such as graphene, graphite, fullerenes, and carbon nanotubes,[36−43] as well as other postgraphene materials such as black phosphorus or molybdenum disulfide.[44−47] Its advantages in terms of an increase in reactivity and in yield of the reaction have been demonstrated by several studies of interest,[48,49] paving the way for the translation of this approach to CNOs. To the best of our knowledge, only a few studies suggest the possibility of CNOs intercalation, but without unambiguous demonstration.[30,50] In one case, Molina-Ontoria *et al.* showed the functionalization of CNOs after a liquid Na/K activation.[30] But only Šiller and co-workers have specifically investigated this intercalation compound with potassium by XPS spectroscopy[50] showing that potassium-treated CNOs behave as a graphite nanocrystal (closer to graphene) instead of exhibiting a molecular behavior despite their molecular-fullerene-like structure. Moreover, by means of carbon dioxide treatment at 1020 K, the CNO structure is damaged and further opened, derived from partial oxidation that creates pores to foster the intercalation.[51] Herein, to pursue the understanding of the intercalation mechanism and final properties, CNO powder was intercalated with metallic potassium at 180 °C for 3 days under an Argon atmosphere (K-CNOs) (Figure 1a, see the

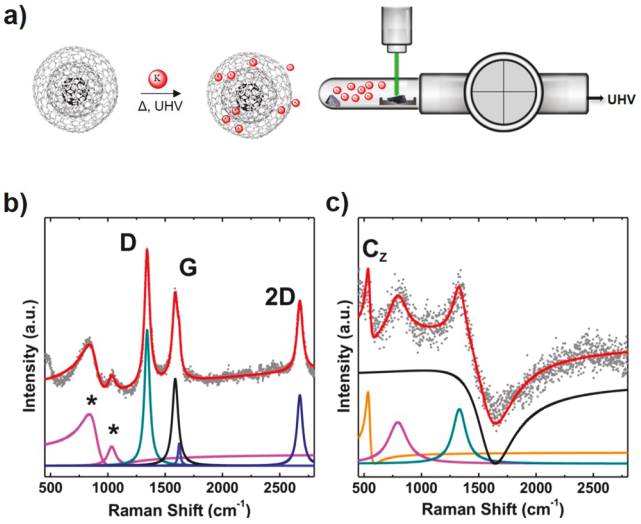

Figure 1. In situ Raman spectra recorded under high-vacuum conditions (~10^{-6} mbar) on intercalated CNOs and their Raman spectra (λ_{ex} = 532 nm). (a) Scheme of the intercalation reaction and the instrumental setup. (b) Deconvolution of Raman spectra of pristine CNOs that are vacuum sealed. Asterisks (pink lines) indicate characteristic glass tube signals. D (1354 cm^{-1}), G (1575 cm^{-1}), and 2D (~2680 cm^{-1}) bands characteristic for CNOs depicted in green, black, and blue, respectively. (c) Deconvolution of Raman spectra of K-CNOs. The Raman spectral lines from pristine CNOs evolve along intercalation into: C_Z band (orange line ~500 cm^{-1}), glass tube peak (pink line), D (green line), and Fano-like G (black).

Supporting Information (SI) for a detailed procedure). The ratio between K and carbon atoms was about 1:8, following a similar procedure reported to be the optimal ratio for KC_8 GICs.[39] Similar to the case of GICs, high temperature and mechanical mixing of the powder are aimed to promote the intercalation of K between the shells of a single onion. It is worth mentioning that the intercalation should proceed through lattice defects on the surface of the CNOs (*vide infra*). The analysis of intercalated CNOs needs to be assessed *in situ*, and due to the high reactivity of this species special controlled conditions for the analysis are required. With this intention, K-CNOs were vacuum-sealed in glass vials, allowing the transportation and the direct analysis of the intercalated compound. *In situ* Raman analysis was performed at different times to follow the occurring change (Figure 1b). Raman spectra of pristine CNOs are typically composed of D (1354 cm^{-1}), G (1575 cm^{-1}), and 2D (~2680 cm^{-1}) bands (Figure 1b, red line) and evolve with intercalation time (Figures 1c and S3). The G band decreases in intensity, while the 2D band disappears after 72 h. This effect is a characteristic feature of highly doped regimes present in the carbon allotrope, which blocks the possibility of having a double resonance process.[52] In addition, a new peak appeared at ~500 cm^{-1} (Figure 1c, red line). This new peak, the so-called C_Z band highlighted by the orange line in the deconvoluted spectra of K-CNOs (Figure 1c), is characteristic for potassium intercalated multiwalled carbon nanotubes (MWNTs)[36] and KC_8 graphite (537 to 565 cm^{-1} respectively).[53] This peak arises from the out-of-plane vibration of the graphitic carbon atoms and only becomes Raman active under intercalation, when the K atoms impose a superstructure within the carbon lattice.[36] Conspicuously, the G line exhibits a Fano resonance formation (Figure 1c, black line) associated with electron−phonon couplings between the

https://doi.org/10.1021/jacs.1c07604
J. Am. Chem. Soc. 2021, 143, 18997−19007

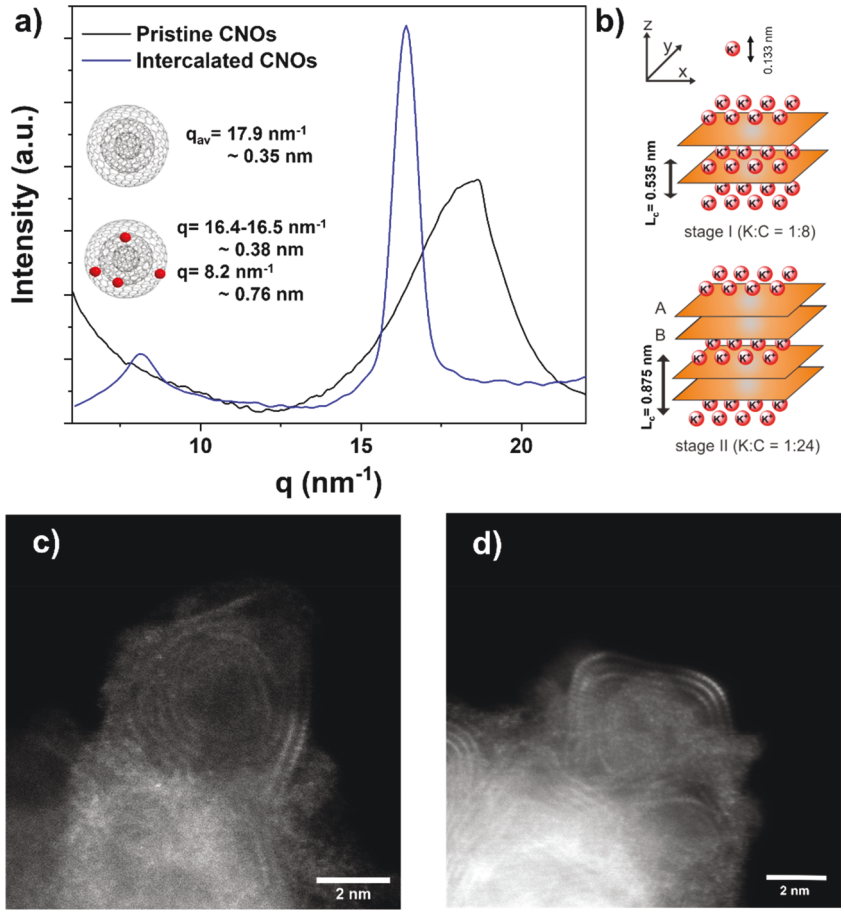

Figure 2. (a) X-ray powder diffraction of pristine and intercalated K-CNOs. Pristine CNOs (black line) are characterized by a broad peak with interlayer distance of ~0.35 nm ($q_{average}$= 17.9 nm^{-1}). K-CNOs (blue line) characterized by two major peaks corresponding to interlayer distances of ~0.38 and ~0.76 nm (q = 8.2 and 16.4 nm^{-1}) are shown. (b) Top: scheme of stage I intercalation compound corresponding to K:C = 1:8. Bottom: stage II intercalation compound, corresponding to K:C = 1:24. (c) STEM-MAADF image of pristine CNOs. (d) STEM-MAADF image of intercalated K-CNOs.

K atoms and the graphitic structure originating from the in-plane E_{2g}^1 vibration of the carbon atoms.[54,55] As observed in Figure 1c, the G-line in the CNOs turned from a Lorentzian line into a Fano-like shape. This effect results from introducing a high concentration of K within the lattice structure of the CNOs. The Fano resonance is a characteristic signature from a highly doped potassium intercalated compound as it has been shown from a stage I GIC KC_8 in MWCNTs KC_8.[36] In addition, it is highly important to consider that an asymmetric Fano line shape of the G-line originates from the strong electron phonon-coupling existing between the K atoms and the graphitic structure of the fullerene and other intercalation compounds. The strong electron phonon-coupling in graphitic based intercalation compounds is a signature of a super-conducting potential behavior of the material. In this sense, one can estimate the renormalized electron−phonon scattering line width (γ^{EPC}) by measuring the G-line frequency of the Fano line (ω_G). However, in our case, this is not possible, as the already established values for adiabatic and nonadiabatic phonon frequencies in graphite[56] will not work for fullerenes as the model may have to be restated for this particular nanostructure.

This first analysis is confirming that the intercalation treatment is leading to changes in the CNOs' electronic structure. To further investigate the effects of intercalation in CNOs, we performed a direct observation of the changes in the CNOs structure through XRD and scanning TEM (STEM). All the analyses were performed under vacuum, maintaining the samples under an inert atmosphere to avoid the deintercalation/oxidation of the reduced species (see the SI). XRD analysis of K-CNOs revealed the presence of two dominant interlayer distances, 0.38 and 0.76 nm (Figure 2a). The first value is close to the one of conventional graphite/graphitic carbon but slightly higher than that observed for the pristine CNOs (~0.35 nm). The second value of *ca.* 0.76 nm reflects the potassium-intercalated onion shells. Comparing this with the family of GICs, the interlayer distance roughly suggests a stage II compound rather than a conventional stage I compound. Specifically, stage I, where the interlayer distance is ~0.535 nm and corresponding to a ratio between K:C = 1:8 (Figure 2b, top), and stage II, in which ~0.875 nm corresponds to a ratio of K:C = 1:24, with the coexistence of two interlayer distances: intercalated and nonintercalated ones (Figure 2b, bottom). Additionally, the formation of Daumas−Hérold type defects cannot be ruled out.[57] The increase of the interlayer distance is a first suggestion of the occurrence of a potassium intercalation, due to the penetration of the metal between the shells. Moreover, the comparison with GICs is suggesting that not all the potassium employed for the intercalation penetrates inside the onions, from which an interlayer distance that lies in between KC_8 and KC_{24} is obtained.[58−60] This phenomenon could be explained by the

https://doi.org/10.1021/jacs.1c07604
J. Am. Chem. Soc. 2021, 143, 18997−19007

difficulty for potassium to enter the first shell of CNOs, which can only occur via defects, and then diffuse between the other inner shells.

To gain further insights into the structure and morphology of the intercalated CNOs, all samples were characterized using the aberration corrected Nion UltraSTEM 100 dedicated scanning transmission electron microscope in Vienna. The intercalated samples were transported in an inert atmosphere and placed on sample holders inside an argon glovebox. They were then moved in the argon atmosphere to the vacuum system connected to the microscope.[61] Pristine samples were transferred through air. All images were recorded with an acceleration voltage of 60 kV using the medium angle annular dark field (MAADF) detector. Based on a statistical analysis of STEM-MAADF images (similar to the ones shown in Figure 2c), the average number of shells is around six. Interestingly, instead of being round, the onions typically exhibited ellipsoidal shapes with different degrees of polygonization, which is also observed for CNO obtained by computer models (*vide infra*). These modifications of the structure can locally affect the interlayer distance which plays an important role in the intercalation. There was no apparent difference in the shape of the onions after the intercalation (see Figure 2d for an example), suggesting that, if potassium enters the onions shells, it does not disrupt the layered structure.

Despite *Z*-contrast, the STEM-MAADF images did not allow us to unambiguously locate potassium within the structures. Therefore, we also employed electron energy loss spectroscopy and spectral mapping within the same instrument. A spectral map of a larger nano-onion is shown in Figure 3a (each pixel shows the total intensity of the spectrum recorded at that location, which roughly corresponds to a *Z*-contrast image). The spectra were recorded with a dispersion of *ca.* 0.33 eV/pixel (512 pixels in total) and were centered at 300 eV. Figure 3b shows a map where the original spectrum map was binned from 256 × 256 to 11 × 11 pixels, and for each pixel the signal corresponding to an energy window of 293−297 eV was divided by that from 289−293 eV (pixels with very low signal corresponding to vacuum were set to zero). As can be seen from the spectra in Figure 3c, that correspond to the marked locations in Figure 3a, the first energy window (pink shaded area) contains both potassium peaks K-L_2 and K-L_3,whereas the second energy window (light blue shaded area) corresponds to the σ^* peak of the carbon K edge. Correspondingly, the red areas in Figure 3b (mostly between the outer layers of the onion) correlate to locations with a high potassium concentration. Notably, in several of the shown spectra, the two potassium peaks are clearly visible (for example, in 3, 4, 8, 9, 10 and 11) despite the overlap with the carbon K peak. Overall, these results support the observation of partial intercalation of CNOs. Additionally, as previously shown by XRD analysis, EELS also suggests an intercalation ratio K:C closer to 1:24, with the remaining potassium being free around the onions.

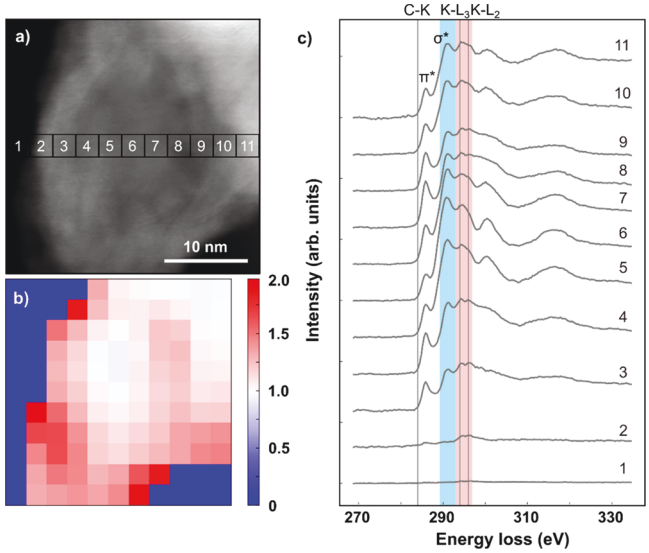

Figure 3. Electron energy loss spectroscopy analysis of an intercalated nano-onion (K-CNO). (a) Spectrum image with each pixel having the intensity corresponding to the sum of the spectrum recorded there leading essentially to thickness contrast. (b) A 11 × 11 pixel map made from the spectrum image of panel (a) by binning the spectra and dividing the integrated intensity within an energy window of 293−297 eV with the intensity from 289−293 eV (except for pixels recorded in vacuum). The energy windows are marked with shaded areas in panel (c). (c) Averaged spectra from the areas marked in panel (a) with numbered squares. Potassium L_3 and L_2 peaks are at 294 and 296 eV (inside the pink shaded area), whereas the C-K σ^* peak is within the second energy window (area shaded light blue).

Once the intercalation of potassium in CNOs has been demonstrated, we used DFT computer models to explore the different energetics of the intercalation process. For this, we simulated the transition states for insertion of K through polyaromatic hydrocarbons with central rings of increasing sizes ranging from 6 to 10 as well as inside a C_{60} fullerene, Figure 4. The activation energy was computed at the M06-2X-6-31G(d) level with the Gaussian09 software.[62]

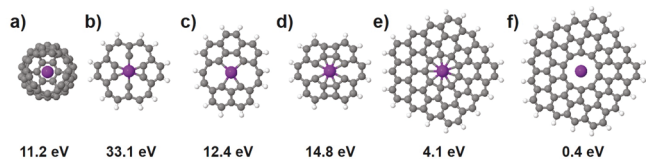

Figure 4. Transition states and corresponding activation energies of K entering C_{60} (a) and trespassing coronene (b), heptacoronene (c), and circulenes with a central octagon (d), nonagon (e), and decagon (f).

The comparison of the mechanism and the energies between the insertion through coronene (33 eV) and fullerene C_{60} (11 eV) through a window opening mechanism is illustrative of how the different curvature and local bonding structures might play a significant role on the activation energy, especially for smaller rings. Nevertheless, these results indicate that only, for relatively large pores, with rings of ≥10 bonds and 0.48 nm in diameter, the insertion barrier for K is low enough (0.4 eV) for the process to proceed at low temperatures.

As previously mentioned, CNOs are often reported as spherical particles, due to their matryoshka-like structure, similar to fullerenes. In contrast, STEM images show different structures such as deformed spheres or ellipsoids. The origin of these modifications remains unclear and has been traditionally attributed to either defects, tension, chemical bond distribution, dimension of the onions, or even temporary deformations as a consequence of the "breathing" of the structures under the electron beam.[63] To better understand this observation, we carried out a computational study where we, through simulated annealing dynamics, transformed 40 different all-carbon

https://doi.org/10.1021/jacs.1c07604
J. Am. Chem. Soc. 2021, 143, 18997−19007

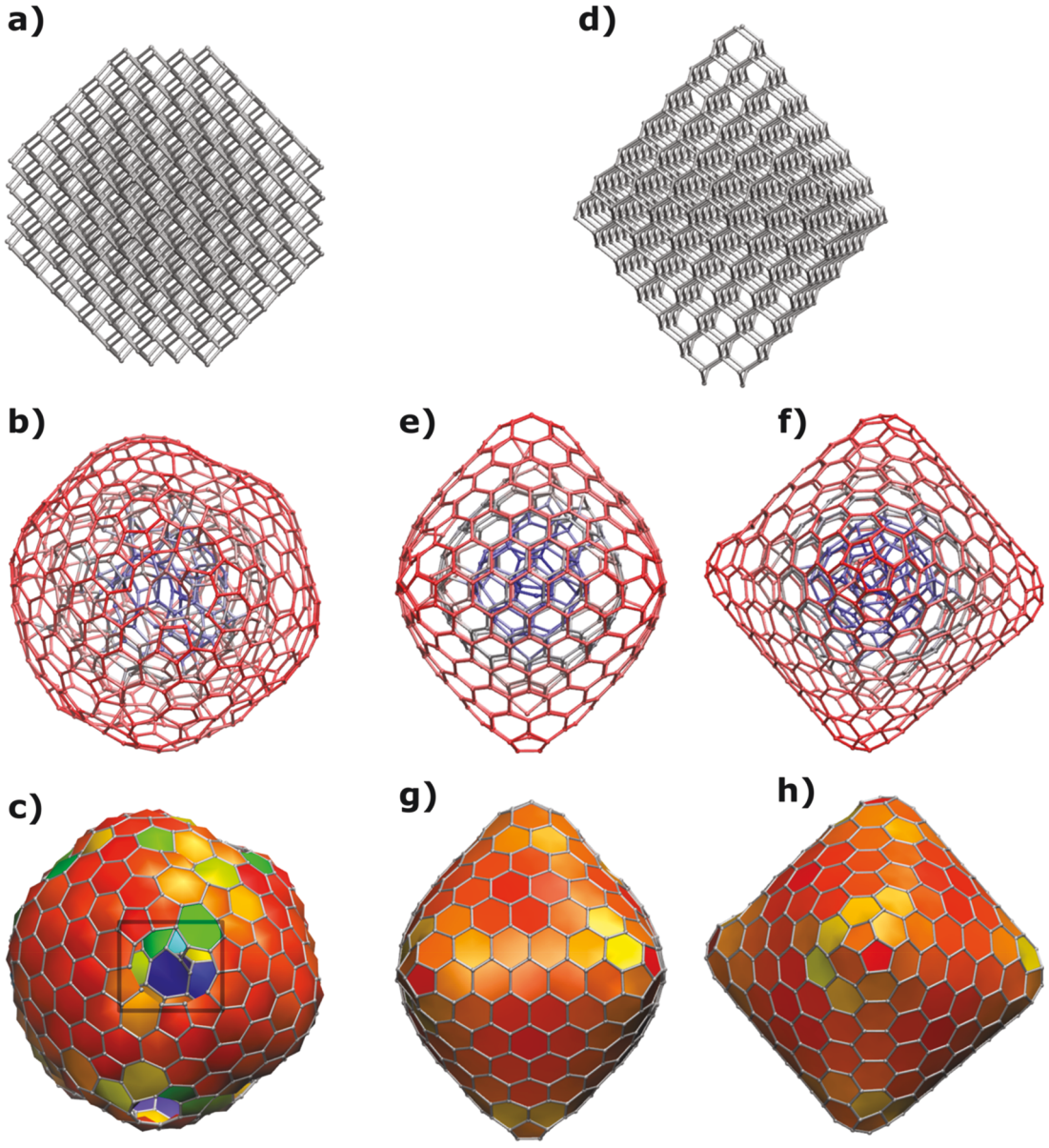

Figure 5. Transformation from nanodiamond to three layer CNOs through simulated annealing. C_{753} nanodiamond (a) and three-layer CNO in two representations (b, c) and C_{674} nanodiamond (d) and three-layer CNO in two representations and two perspectives (e−h). The rectangle in C_{753} CNO (c) serves to highlight the undecagon hole on the CNO surface.

nanodiamond particles ranging from C_{35} to C_{969} to CNOs.[64] For this, simulations were run with the Brenner bond order potential implemented in a home version of the TINKER code during 2 ns runs with linearly increasing temperatures from 1300 to 3500 K.[65] Here, 2000 snapshots were taken from each dynamic trajectory and subsequently minimized to find the most thermodynamically stable nanoparticle for each system. In the last step, the so-obtained molecular structures were minimized with the GFN2 extended tight-binding methodology which allows for the efficient computation of large molecular systems with quantum mechanical Hamiltonians.[66]

Two representative systems comprising a pseudospherical CNO, C_{753}, and a polygonal one, C_{674}, were selected and will be discussed comparatively. In both cases, the transformation started by reconstructing the external, and more undercoordinated, region of the initial nanoparticles. The pure octahedral C_{674} nanodiamond kept its regular shape, while the truncated octahedral C_{753} nanodiamond transformed into a pseudospherical CNO (Figure 5). This difference was also reflected by the different simulated annealing temperatures needed: 2093 and 2804 K, respectively. Interestingly, the C_{674} CNO shows a nearly octahedral shape with a defect-free external shell composed exclusively of hexagons and pentagons matching what is found in most fullerenes. In contrast, C_{753} CNO possesses an irregular pseudospherical shape with pentagons, hexagons, and heptagons together with some larger holes with sizes up to undecagons which would be the most likely entry point in this case for the K in the intercalation mechanism. Altogether, these findings confirm the suggestion by Šiller and co-workers that the intercalation of CNOs occurs due to the presence of surface defects, as a result of the synthetic CNO preparation, and strongly support the experimental results shown here.[50,63]

https://doi.org/10.1021/jacs.1c07604
J. Am. Chem. Soc. 2021, 143, 18997−19007

Finally, to prove the efficiency of the potassium intercalation strategy, K-CNOs were functionalized using two reactive species, hexyl iodide and phenyl iodide, well-known and investigated for the functionalization of GICs (Scheme 1, SI

Scheme 1. Reaction Scheme of CNO Intercalation (First Step) followed by Functionalization with Hexyl Iodide or Phenyl Iodide (Second Step) and Schematic Representation of Functionalized CNOs

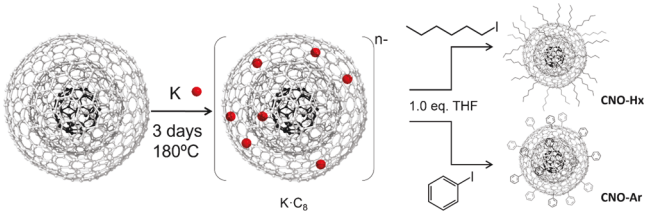

for reaction conditions). Both reagents allow a covalent bulk functionalization with the employment of a low amount of reacting species, avoiding the occurrence of side reactions and the formation of coupling products.[39] Moreover, the choice of well-known reagents allows an easy characterization of the onions due to the simple moieties introduced on their surface.

Differently from classic organic synthesis, the characterization of nanomaterials requires a cross-correlated analysis of several techniques to prove an intended functionalization. Following this line, we evaluated the number of functional groups and their integrity. Raman spectroscopy is one of the most commonly employed techniques to analyze modifications on the nanomaterials lattice.[67−69] Similar to graphene, Raman bands such as the D band (∼1350 nm), G band (∼1580 nm), and 2D band (∼2680 nm) are characteristic for CNOs. In contrast to graphene, in which the information about functionalization, number of layers, and surface change can easily be extracted, for CNOs, the presence of an intense D band makes a precise estimation of the I_D/I_G ratio quite difficult. Moreover, the analysis of hundreds of single point spectra of pristine CNOs reveals a broad distribution of I_D/I_G ratios ranging from *ca.* 1.1 to 1.4, pointing out the importance of a statistical assessment for the correct interpretation of the functionalization reactions. Indeed, D and G band intensities are very close for onions synthesized by thermal annealing, reducing the change on the spectra due to chemical functionalization. Herein, we performed a unique statistical Raman analysis and temperature dependent Raman analysis on functionalized CNOs (f-CNOs) in order to obtain an accurate estimation of the functionalization reaction. Areas of 10 μm were analyzed, obtaining more than 200 points for the pristine material and more than 600 points for f-CNOs. Figure 6 shows the results of the I_D/I_G ratio and I_{2D}/I_G ratio. The average values of the pristine and the f-CNOs do not show a highly significant difference, with 1.23 ± 0.0002, 1.30 ± 0.0009, and 1.37 ± 0.0010, respectively, for pristine, hexyl, and aryl functionalized onions (see Figure 6, table). However, clear evidence of the functionalization that occurred is shown by the I_D/I_G and I_{2D}/I_G ratio distribution. The first column shows a shift on the I_D/I_G ratio distribution for both hexyl and aryl

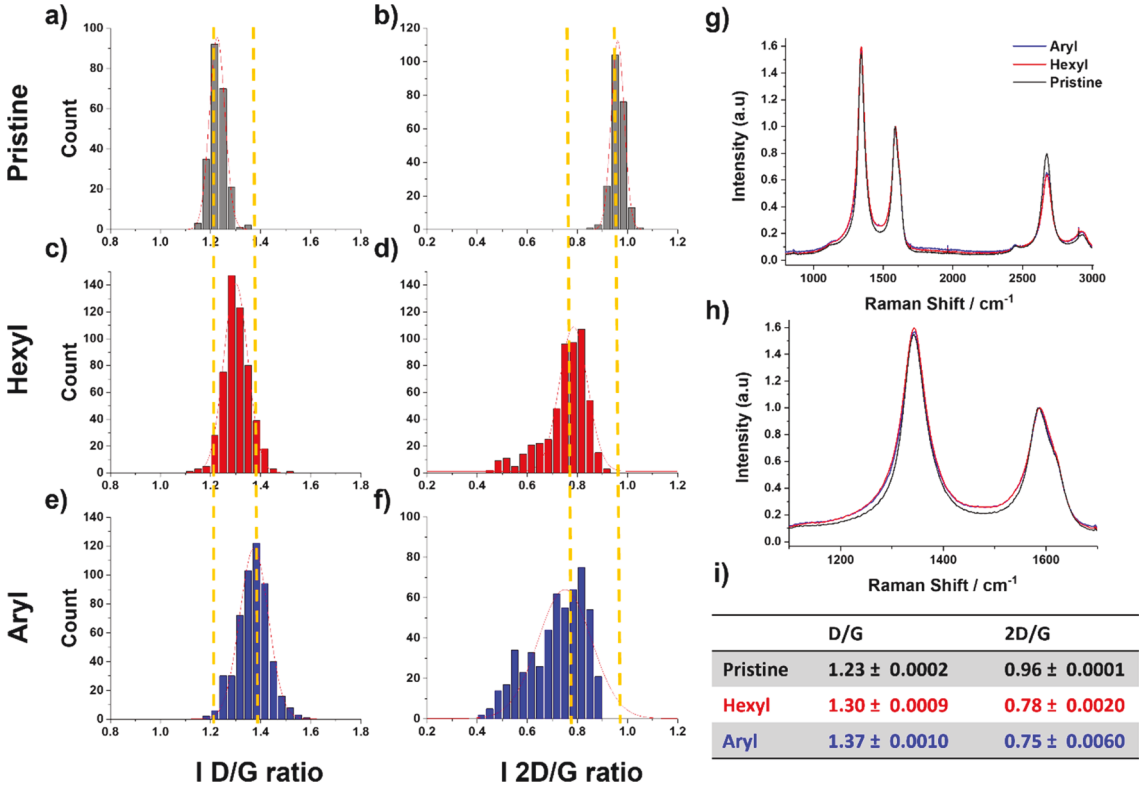

	D/G	2D/G
Pristine	1.23 ± 0.0002	0.96 ± 0.0001
Hexyl	1.30 ± 0.0009	0.78 ± 0.0020
Aryl	1.37 ± 0.0010	0.75 ± 0.0060

Figure 6. Statistical Raman analysis performed on a 10 μm surface area. First row: Pristine CNOs, 200 points collected for each map., (a) I_D/I_G ratio and (b) I_{2D}/I_G ratio. Second row: Hexyl functionalized CNOs, 625 single points collected, (c) I_D/I_G ratio and (d) I_{2D}/I_G ratio. Third row: Aryl functionalized CNOs, 625 single points collected, (e) I_D/I_G ratio and (f) I_{2D}/I_G ratio. (g) Comparison of the mean Raman spectra from the Raman mapping, CNOs pristine (black line), CNOs-hexyl (red line), and CNO-aryl (blue line). (h) Higher magnification of the Raman spectra shown in (g) . (i) Table summarizing the I_D/I_G ratio and I_{2D}/I_G ratio.

https://doi.org/10.1021/jacs.1c07604
J. Am. Chem. Soc. 2021, 143, 18997−19007

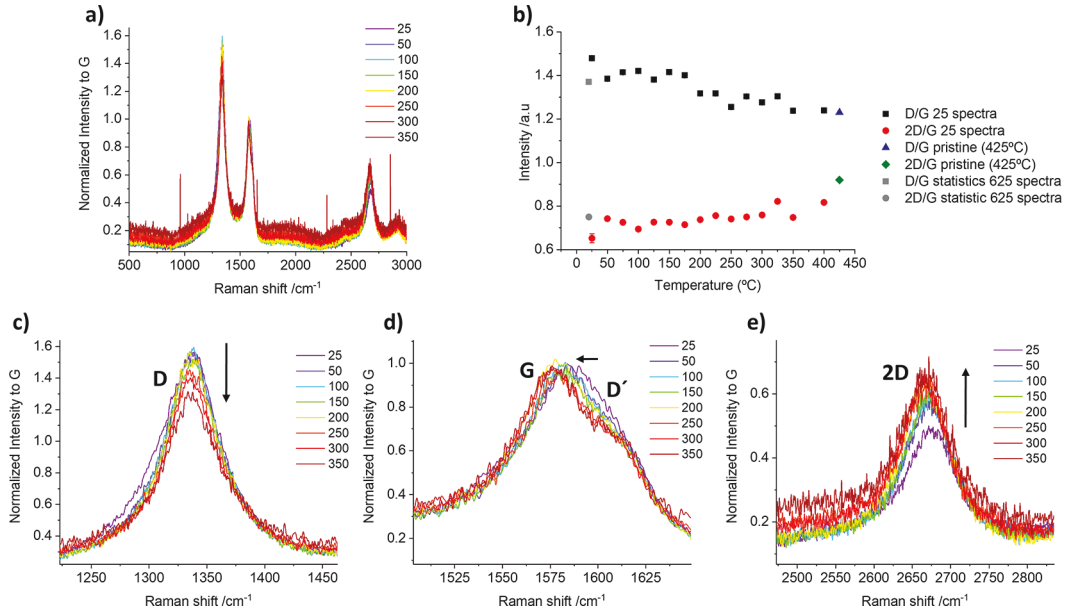

Figure 7. Temperature-dependent Raman analysis of CNOs-aryl. (a) Stacking of Raman spectra from 25 to 350 °C. (b) Evolution of the I_D/I_G and I_{2D}/I_G ratios with increasing temperature. The ratios of the statistical map for pristine CNOs (represented by the blue triangle and the green rhombus) at 425 °C are recovered after the thermal defunctionalization treatment. (c) Magnification of CNOs D band; the decrease of D band intensity with increasing temperatures is highlighted by a black arrow. (d) Magnification of CNOs G and D′ bands, showing D′ disappearance with increasing temperatures. (e) Magnification of CNOs 2D band, showing the increase of 2D band intensity with increasing temperatures.

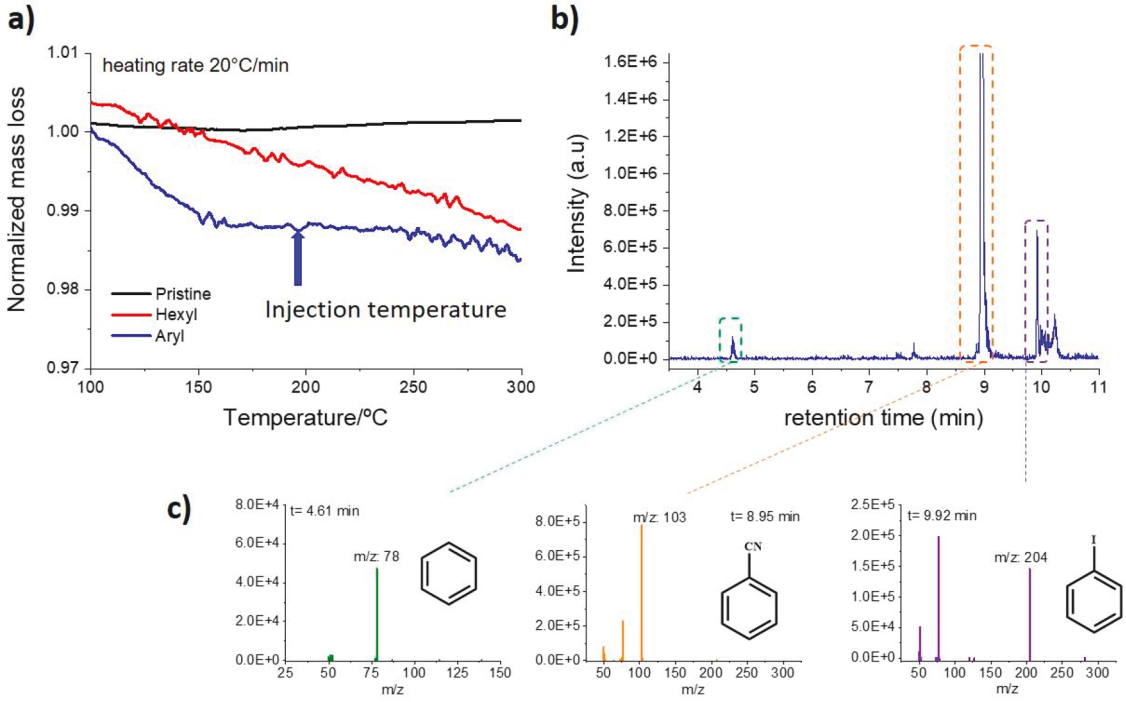

Figure 8. TGA-GC-MS analysis from CNOs-aryl. (a) TGA profile of CNO-aryl (blue line); blue arrow indicates sample injection at 200 °C during TGA analysis. (b) CNOs-aryl GC chromatogram; peaks marked with a colored box are relative to fragments from functional groups. (c) MS fragment analysis of GC peaks at 4.61, 8.95, and 9.92 min. Residual benzonitrile presence from the workup protocol is shown by the peak at ∼8.95 min.

functionalized CNOs compared to the pristine onions, with an increase of the intensity of the D band, typically attributed to the functionalization of carbon nanomaterials. Accordingly, the I_{2D}/I_G ratio of functionalized CNOs shows a significant shift to lower values and broadening with respect to the pristine one. These observations highlight the importance of the statistical Raman analysis for the characterization of nanomaterials. In fact, from the simple comparison of the average Raman spectra (Figure 6g, h), the information about the intensity ratio would have been lost, resulting in the misleading conclusion that no reaction occurred on the material. Additionally, the analysis of

https://doi.org/10.1021/jacs.1c07604
J. Am. Chem. Soc. 2021, 143, 18997−19007

few Raman spectra could have led to errors as well, because of the low number of cases analyzed.

Furthermore, we performed a temperature-dependent Raman analysis, from 0 to 425 °C, to investigate the reversibility in the functionalization of CNOs. This technique was already employed by our group to understand the response of functional groups and nanomaterials to temperature.[39,48,70] Starting from 0 °C, a Raman map was collected by 25 °C steps. In this case, the scanning and warming time was minimized, performing maps of 25 single points each, to avoid the prolonged warming of the sample at high temperatures. The results are depicted in Figure 7 for CNOs-aryl (Figures S4 and S5 for pristine and CNOs-hexyl, respectively). A concomitant narrowing and decrease of the D band upon defunctionalization and an increase of intensity of the 2D band, corroborating the defunctionalization due to the increase of the temperature, were observed. Furthermore, the disappearance of the D′ shoulder at around 1620 cm^{-1} is observed upon heating. Finally, and perhaps most importantly, the recovery of the pristine CNOs' I_D/I_G ratio after thermal treatment demonstrates that the carbon lattice is not damaged during the reduction or the functionalization process. A reference map analysis on pristine CNOs was also performed to discard possible effects due to temperature. As expected, no significant changes in the Raman spectra were found.

To analyze the fragments of the organic molecules detached from the samples upon heating, a special technique based on the coupling of thermogravimetric analysis, gas chromatography, and mass-spectrometry (TGA/GC/MS) was performed. This technique is known for its efficacy in the characterization of other carbon nanomaterials, even in the presence of multiple functional groups.[70] Several advantages arise from the combination of these techniques: first, the possibility of choosing the temperature at which to analyze the gas developed and the precise separation of the components through gas chromatography. Second, the high sensitivity of mass spectrometry and cross-reference with mass-fragmentation libraries allow a deep understanding of the composition of each eluted compound, in direct correlation to the defunctionalization of the materials. Initially, simple TGA analysis was carried out (Figure 8a and entire TGA profile in Figure S6a), showing the high stability of pristine CNOs up to a temperature of 700 °C. The CNO-hexyl presents a constant weight loss starting from a temperature of ∼120 °C, while CNO-aryl presents a more marked weight loss at ∼140 °C and then from 200 °C (Figure S6b). Therefore, we collected and analyzed the gas produced at 200 °C for CNO-aryl (Figure 8b) and 180 °C for CNOs-hexyl (Figure S7b). The CNO-aryl sample presents the main peak of benzene after 4.61 min, corresponding to m/z of 78 (Figure 8c). Together, at 9.92 min, a peak corresponding to unreacted iodobenzene is present (m/z = 204). A similar behavior was observed by the CNO-Hexyl sample, with three main peaks at 4.14, 4.18, and 5.99 min (Figure S7c). The fragmentation analysis corresponds to different fragments arising from the hexyl chain during the warming of the materials. A similar behavior was shown by conventional TGA-MS direct analysis performed on CNO-hexyl (Figure S8b). The temperature/ion current spectra show three main fragments formed at ∼300 °C during heating of the CNOs. The m/z fragments of 43, 57, and 86 correspond to linear aliphatic compounds from C_3H_7, C_4H_9, and C_3H_7−CO−CH_2^+. The high temperature at which the fragments are detected (>300 °C) confirms their origin as a functional group of CNOs, discarding adsorbed organic molecules, expected to appear at lower temperatures. Other common characterization techniques such as attenuated total reflectance Fourier-transformed infrared spectroscopy (ATR-FTIR), absorption spectroscopy (UV−vis), and dynamic light scattering (DLS) corroborate our results and can be found in the Supporting Information (see SI Figures S9 and S10).

CONCLUSION

In this study, we carried out a combination of different *in situ* and *ex situ* characterization techniques supported by extensive theoretical calculations. This demonstrates that CNOs can be successfully intercalated with potassium through surface defects by means of thermal heating at relatively low temperatures. Moreover, we developed the reductive covalent functionalization of CNOs with both hexyl iodide and aryl iodide, showing unambiguous spectroscopic fingerprints thanks to the cross-analysis of statistical Raman spectroscopy and TG-GC-MS, among others. This work provides an important insight into the structure of intercalated and functionalized CNOs as well as the understanding of the basic principles of their alkali metal intercalation and reductive functionalization. This work may lay the foundations for future applications of CNOs in which metal intercalation and surface engineering play a crucial role.

ASSOCIATED CONTENT

Supporting Information

The Supporting Information is available free of charge at https://pubs.acs.org/doi/10.1021/jacs.1c07604.

Synthesis of materials, functionalization, characterization techniques, and Raman statistical analysis (PDF)

AUTHOR INFORMATION

Corresponding Authors

M. Eugenia Pérez-Ojeda − *Department of Chemistry and Pharmacy, Chair of Organic Chamistry II, Friedrich-Alexander University of Erlangen-Nuremberg, 91058 Erlangen, Germany; Joint Institute of Advanced Materials and Processes (ZMP), Friedrich-Alexander University of Erlangen-Nuremberg, D-90762 Fürth, Germany;* Email: eugenia.perez-ojeda@fau.de

Luis Echegoyen − *Department of Chemistry, University of Texas at El Paso, El Paso, Texas 79968, United States;* orcid.org/0000-0003-1107-9423; Email: echegoyen@utep.ed

Andreas Hirsch − *Department of Chemistry and Pharmacy, Chair of Organic Chamistry II, Friedrich-Alexander University of Erlangen-Nuremberg, 91058 Erlangen, Germany; Joint Institute of Advanced Materials and Processes (ZMP), Friedrich-Alexander University of Erlangen-Nuremberg, D-90762 Fürth, Germany;* orcid.org/0000-0003-1458-8872; Email: andreas.hirsch@fau.de

Gonzalo Abellán − *Instituto de Ciencia Molecular, Universidad de Valencia, 46980 Paterna, Spain;* orcid.org/0000-0003-1564-6210; Email: gonzalo.abellan@uv.es

Authors

Edison Castro − *Department of Chemistry, University of Texas at El Paso, El Paso, Texas 79968, United States*

Claudia Kröckel − *Department of Chemistry and Pharmacy, Chair of Organic Chamistry II, Friedrich-Alexander University of Erlangen-Nuremberg, 91058 Erlangen, Germany; Joint Institute of Advanced Materials and Processes (ZMP), Friedrich-Alexander University of Erlangen-Nuremberg, D-90762 Fürth, Germany;* orcid.org/0000-0001-5149-9540

Matteo Andrea Lucherelli − *Instituto de Ciencia Molecular, Universidad de Valencia, 46980 Paterna, Spain;* orcid.org/0000-0003-1055-3269

Ursula Ludacka − *Faculty of Physics, University of Vienna, 1090 Vienna, Austria*

Jani Kotakoski − *Faculty of Physics, University of Vienna, 1090 Vienna, Austria;* orcid.org/0000-0002-1301-5266

Katharina Werbach − *Faculty of Physics, University of Vienna, 1090 Vienna, Austria*

Herwig Peterlik − *Faculty of Physics, University of Vienna, 1090 Vienna, Austria*

Manuel Melle-Franco − *CICECO-Aveiro Institute of Materials, Department of Chemistry, University of Aveiro, 3810-193 Aveiro, Portugal;* orcid.org/0000-0003-1929-0477

Julio C. Chacón-Torres − *School of Physical Sciences and Nanotechnology, Yachay Tech University, 100119 Urcuquí, Ecuador;* orcid.org/0000-0002-1833-504X

Frank Hauke − *Department of Chemistry and Pharmacy, Chair of Organic Chamistry II, Friedrich-Alexander University of Erlangen-Nuremberg, 91058 Erlangen, Germany; Joint Institute of Advanced Materials and Processes (ZMP), Friedrich-Alexander University of Erlangen-Nuremberg, D-90762 Fürth, Germany;* orcid.org/0000-0001-9637-7299

Complete contact information is available at: https://pubs.acs.org/10.1021/jacs.1c07604

Notes

The authors declare no competing financial interest.

■ ACKNOWLEDGMENTS

The work was supported by the European Union (ERC Advanced Grant 742145 B-PhosphoChem to A.H., ERC-2018-StG 804110-2D-PnictoChem to G.A.), the German Research Foundation (DFG) (Project-ID 182849149 SFB 953 "Synthetic Carbon Allotropes" project A1 (A.H.), project A9 (M.E.P.-O.), as well as FLAG-ERA AB694/2-1 (G.A.)), and the Spanish MICINN (PID2019-111742GA-I00, "María de Maeztu" Program for Units of Excellence in R&D CEX2019-000919-M). G.A. acknowledges support by the Generalitat Valenciana (CIDEGENT/2018/001 and iDiFEDER/2018/061 cofinanced by FEDER). M.E.P.-O. acknowledges support by "Emerging Talents Initiative (ETI)" from Friedrich-Alexander Universität Erlangen-Nürnberg. M.M.-F. acknowledges support through the project IF/00894/2015 and within the scope of the project CICECO-Aveiro Institute of Materials, UIDB/50011/2020 & UIDP/50011/2020 funded by national funds through the Portuguese Foundation for Science and Technology I.P./MCTES. In addition, the research leading to these results has received partial funding from the European Union Seventh Framework Program under Grant Agreement No. 604391 Graphene Flagship. L.E. and E.C. would like to thank the US NSF for the generous support of this work under CHE-1801317 and to the Robert A. Welch Foundation for an endowed chair to L.E. (Grant AH-0033).

■ REFERENCES

(1) Kroto, H. W.; Heath, J. R.; O'Brien, S. C.; Curl, R. F.; Smalley, R. E. C60 : Buckminsterfullerene. *Nature* **1985**, *318* (6042), 162−163.

(2) Bepete, G.; Anglaret, E.; Ortolani, L.; Morandi, V.; Huang, K.; Pénicaud, A.; Drummond, C. Surfactant-Free Single-Layer Graphene in Water. *Nat. Chem.* **2017**, *9* (4), 347−352.

(3) Pénicaud, A.; Drummond, C. Deconstructing Graphite: Graphenide Solutions. *Acc. Chem. Res.* **2013**, *46* (1), 129−137.

(4) Ugarte, D. Curling and Closure of Graphitic Networks under Electron-Beam Irradiation. *Nature* **1992**, *359* (6397), 707−709.

(5) Iijima, S. Direct Observation of the Tetrahedral Bonding in Graphitized Carbon Black by High Resolution Electron Microscopy. *J. Cryst. Growth* **1980**, *50* (3), 675−683.

(6) Dhand, V.; Yadav, M.; Kim, S. H.; Rhee, K. Y. A Comprehensive Review on the Prospects of Multi-Functional Carbon Nano Onions as an Effective, High-Performance Energy Storage Material. *Carbon* **2021**, *175*, 534−575.

(7) Pech, D.; Brunet, M.; Durou, H.; Huang, P.; Mochalin, V.; Gogotsi, Y.; Taberna, P.-L.; Simon, P. Ultrahigh-Power Micrometre-Sized Supercapacitors Based on Onion-like Carbon. *Nat. Nanotechnol.* **2010**, *5* (9), 651−654.

(8) Xu, J.; Chen, X.; Grützmacher, P.; Rosenkranz, A.; Li, J.; Jin, J.; Zhang, C.; Luo, J. Tribochemical Behaviors of Onion-like Carbon Films as High-Performance Solid Lubricants with Variable Interfacial Nanostructures. *ACS Appl. Mater. Interfaces* **2019**, *11* (28), 25535−25546.

(9) Street, K. W.; Marchetti, M.; VanderWal, R. L.; Tomasek, A. J. Evaluation of the Tribological Behavior of Krytox 143AB with Nano-Onions. *NTRS - NASA Technical Reports Server*; NASA/TM-2003-212301; 2003; pp 1−9.

(10) Bartelmess, J.; De Luca, E.; Signorelli, A.; Baldrighi, M.; Becce, M.; Brescia, R.; Nardone, V.; Parisini, E.; Echegoyen, L.; Pompa, P. P.; Giordani, S. Boron Dipyrromethene (BODIPY) Functionalized Carbon Nano-Onions for High Resolution Cellular Imaging. *Nanoscale* **2014**, *6* (22), 13761−13769.

(11) Camisasca, A.; Giordani, S. Carbon Nano-Onions in Biomedical Applications: Promising Theranostic Agents. *Inorg. Chim. Acta* **2017**, *468*, 67−76.

(12) Mykhailiv, O.; Zubyk, H.; Plonska-Brzezinska, M. E. Carbon Nano-Onions: Unique Carbon Nanostructures with Fascinating Properties and Their Potential Applications. *Inorg. Chim. Acta* **2017**, *468*, 49−66.

(13) Bartelmess, J.; Quinn, S. J.; Giordani, S. Carbon Nanomaterials: Multi-Functional Agents for Biomedical Fluorescence and Raman Imaging. *Chem. Soc. Rev.* **2015**, *44* (14), 4672−4698.

(14) Plonska-Brzezinska, M. E. Carbon Nano-Onions: A Review of Recent Progress in Synthesis and Applications. *ChemNanoMat* **2019**, *5* (5), 568−580.

(15) Yang, J.; Kim, S. H.; Kwak, S. K.; Song, H.-K. Curvature-Induced Metal−Support Interaction of an Islands-by-Islands Composite of Platinum Catalyst and Carbon Nano-Onion for Durable Oxygen Reduction. *ACS Appl. Mater. Interfaces* **2017**, *9* (28), 23302−23308.

(16) Huang, J. Y.; Yasuda, H.; Mori, H. Highly Curved Carbon Nanostructures Produced by Ball-Milling. *Chem. Phys. Lett.* **1999**, *303* (1), 130−134.

(17) Cabioc'h, T.; Riviere, J. P.; Delafond, J. A New Technique for Fullerene Onion Formation. *J. Mater. Sci.* **1995**, *30* (19), 4787−4792.

(18) Sano, N.; Wang, H.; Chhowalla, M.; Alexandrou, I.; Amaratunga, G. a. J. Synthesis of Carbon "onions" in Water. *Nature* **2001**, *414* (6863), 506−507.

(19) Du, A.-B.; Liu, X.-G.; Fu, D.-J.; Han, P.-D.; Xu, B.-S. Onion-like Fullerenes Synthesis from Coal. *Fuel* **2007**, *86* (1), 294−298.

(20) Chen, X. H.; Deng, F. M.; Wang, J. X.; Yang, H. S.; Wu, G. T.; Zhang, X. B.; Peng, J. C.; Li, W. Z. New Method of Carbon Onion

Growth by Radio-Frequency Plasma-Enhanced Chemical Vapor Deposition. *Chem. Phys. Lett.* **2001**, *336* (3), 201−204.
(21) Dorobantu, D.; Bota, P. M.; Boerasu, I.; Bojin, D.; Enachescu, M. Pulse Laser Ablation System for Carbon Nano-Onions Fabrication. *Surf. Engin. Appl.Electrochem.* **2014**, *50* (5), 390−394.
(22) Roddatis, V. V.; Kuznetsov, V. L.; Butenko, Yu. V.; Su, D. S.; Schlögl, R. Transformation of Diamond Nanoparticles into Carbon Onions under Electron Irradiation. *Phys. Chem. Chem. Phys.* **2002**, *4* (10), 1964−1967.
(23) Abellán, G.; Coronado, E.; Martí-Gastaldo, C.; Ribera, A.; Sánchez-Royo, J. F. Layered Double Hydroxide (LDH)−Organic Hybrids as Precursors for Low-Temperature Chemical Synthesis of Carbon Nanoforms. *Chem. Sci.* **2012**, *3* (5), 1481−1485.
(24) Abellán, G.; Coronado, E.; Martí-Gastaldo, C.; Ribera, A.; Otero, T. F. Magnetic Nanocomposites Formed by FeNi3 Nanoparticles Embedded in Graphene. Application as Supercapacitors. *Part. Part. Syst. Charact.* **2013**, *30* (10), 853−863.
(25) Guo, A.; Bao, K.; Sang, S.; Zhang, X.; Shao, B.; Zhang, C.; Wang, Y.; Cui, F.; Yang, X. Soft-Chemistry Synthesis, Solubility and Interlayer Spacing of Carbon Nano-Onions. *RSC Adv.* **2021**, *11* (12), 6850−6858.
(26) Kuznetsov, V. L.; Chuvilin, A. L.; Butenko, Y. V.; Mal'kov, I. Yu.; Titov, V. M. Onion-like Carbon from Ultra-Disperse Diamond. *Chem. Phys. Lett.* **1994**, *222* (4), 343−348.
(27) Chen, J.; Deng, S. Z.; Chen, J.; Yu, Z. X.; Xu, N. S. Graphitization of Nanodiamond Powder Annealed in Argon Ambient. *Appl. Phys. Lett.* **1999**, *74* (24), 3651−3653.
(28) Palkar, A.; Melin, F.; Cardona, C. M.; Elliott, B.; Naskar, A. K.; Edie, D. D.; Kumbhar, A.; Echegoyen, L. Reactivity Differences between Carbon Nano Onions (CNOs) Prepared by Different Methods. *Chem. - Asian J.* **2007**, *2* (5), 625−633.
(29) Bartelmess, J.; Giordani, S. Carbon Nano-Onions (Multi-Layer Fullerenes): Chemistry and Applications. *Beilstein J. Nanotechnol.* **2014**, *5*, 1980−1998.
(30) Molina-Ontoria, A.; Chaur, M. N.; Plonska-Brzezinska, M. E.; Echegoyen, L. Preparation and Characterization of Soluble Carbon Nano-Onions by Covalent Functionalization, Employing a Na−K Alloy. *Chem. Commun.* **2013**, *49* (24), 2406−2408.
(31) Morishita, T.; Clancy, A. J.; Shaffer, M. S. P. Optimised Exfoliation Conditions Enhance Isolation and Solubility of Grafted Graphenes from Graphite Intercalation Compounds. *J. Mater. Chem. A* **2014**, *2* (36), 15022−15028.
(32) Englert, J. M.; Dotzer, C.; Yang, G.; Schmid, M.; Papp, C.; Gottfried, J. M.; Steinrück, H. P.; Spiecker, E.; Hauke, F.; Hirsch, A. Covalent Bulk Functionalization of Graphene. *Nat. Chem.* **2011**, *3* (4), 279−286.
(33) Hirsch, A.; Englert, J. M.; Hauke, F. Wet Chemical Functionalization of Graphene. *Acc. Chem. Res.* **2013**, *46* (1), 87−96.
(34) Hof, F.; Bosch, S.; Englert, J. M.; Hauke, F.; Hirsch, A. Statistical Raman Spectroscopy: A Method for the Characterization of Covalently Functionalized Single-Walled Carbon Nanotubes. *Angew. Chem., Int. Ed.* **2012**, *51* (47), 11727−11730.
(35) Englert, J. M.; Vecera, P.; Knirsch, K. C.; Schäfer, R. A.; Hauke, F.; Hirsch, A. Scanning-Raman-Microscopy for the Statistical Analysis of Covalently Functionalized Graphene. *ACS Nano* **2013**, *7* (6), 5472−5482.
(36) Chacón-Torres, J. C.; Dzsaber, S.; Vega-Diaz, S. M.; Akbarzadeh, J.; Peterlik, H.; Kotakoski, J.; Argentero, G.; Meyer, J. C.; Pichler, T.; Simon, F.; Terrones, M.; Reich, S. Potassium Intercalated Multiwalled Carbon Nanotubes. *Carbon* **2016**, *105*, 90−95.
(37) Chacón-Torres, J. C.; Ganin, A. Y.; Rosseinsky, M. J.; Pichler, T. Raman Response of Stage-1 Graphite Intercalation Compounds Revisited. *Phys. Rev. B: Condens. Matter Mater. Phys.* **2012**, *86* (7), 075406.
(38) Knirsch, K. C.; Englert, J. M.; Dotzer, C.; Hauke, F.; Hirsch, A. Screening of the Chemical Reactivity of Three Different Graphite Sources Using the Formation of Reductively Alkylated Graphene as a Model Reaction. *Chem. Commun.* **2013**, *49* (92), 10811−10813.
(39) Abellán, G.; Schirowski, M.; Edelthalhammer, K. F.; Fickert, M.; Werbach, K.; Peterlik, H.; Hauke, F.; Hirsch, A. Unifying Principles of the Reductive Covalent Graphene Functionalization. *J. Am. Chem. Soc.* **2017**, *139* (14), 5175−5182.
(40) Hof, F.; Bosch, S.; Eigler, S.; Hauke, F.; Hirsch, A. New Basic Insight into Reductive Functionalization Sequences of Single Walled Carbon Nanotubes (SWCNTs). *J. Am. Chem. Soc.* **2013**, *135* (49), 18385−18395.
(41) Kröckel, C.; Preciado-Rivas, M. R.; Torres-Sánchez, V. A.; Mowbray, D. J.; Reich, S.; Hauke, F.; Chacón-Torres, J. C.; Hirsch, A. Understanding the Electron-Doping Mechanism in Potassium-Intercalated Single-Walled Carbon Nanotubes. *J. Am. Chem. Soc.* **2020**, *142* (5), 2327−2337.
(42) Wabra, I.; Holzwarth, J.; Hauke, F.; Hirsch, A. Exohedral Addition Chemistry of the Fullerenide Anions C602− and C60·−. *Chem. - Eur. J.* **2019**, *25* (20), 5186−5201.
(43) V. Damasceno, J. P.; Hof, F.; Chauvet, O.; Zarbin, A. J. G.; Pénicaud, A. The Role of Functionalization on the Colloidal Stability of Aqueous Fullerene C60 Dispersions Prepared with Fullerides. *Carbon* **2021**, *173*, 1041−1047.
(44) Abellán, G.; Neiss, C.; Lloret, V.; Wild, S.; Chacón-Torres, J. C.; Werbach, K.; Fedi, F.; Shiozawa, H.; Görling, A.; Peterlik, H.; Pichler, T.; Hauke, F.; Hirsch, A. Exploring the Formation of Black Phosphorus Intercalation Compounds with Alkali Metals. *Angew. Chem., Int. Ed.* **2017**, *56* (48), 15267−15273.
(45) Wild, S.; Dinh, X. T.; Maid, H.; Hauke, F.; Abellán, G.; Hirsch, A. Quantifying the Covalent Functionalization of Black Phosphorus. *Angew. Chem., Int. Ed.* **2020**, *59* (45), 20230−20234.
(46) Werbach, K.; Neiss, C.; Müllner, A.; Abellán, G.; Setman, D.; Lloret, V.; Wild, S.; Hauke, F.; Pichler, T.; Hirsch, A.; Peterlik, H. Controlling the Formation of Sodium/Black Phosphorus IntercalationCompounds Towards High Sodium Content. *Batteries & Supercaps* **2021**, *4*, 1304−1309.
(47) Chen, X.; Denninger, P.; Stimpel-Lindner, T.; Spiecker, E.; Duesberg, G. S.; Backes, C.; Knirsch, K. C.; Hirsch, A. Defect Engineering of Two-Dimensional Molybdenum Disulfide. *Chem. - Eur. J.* **2020**, *26* (29), 6535−6544.
(48) Schirowski, M.; Abellán, G.; Nuin, E.; Pampel, J.; Dolle, C.; Wedler, V.; Fellinger, T. P.; Spiecker, E.; Hauke, F.; Hirsch, A. Fundamental Insights into the Reductive Covalent Cross-Linking of Single-Walled Carbon Nanotubes. *J. Am. Chem. Soc.* **2018**, *140* (9), 3352−3360.
(49) Vecera, P.; Edelthalhammer, K.; Hauke, F.; Hirsch, A. Reductive Arylation of Graphene: Insights into a Reversible Carbon Allotrope Functionalization Reaction. *Phys. Status Solidi B* **2014**, *251* (12), 2536−2540.
(50) Montalti, M.; Krishnamurthy, S.; Chao, Y.; Butenko, Yu. V.; Kuznetsov, V. L.; Dhanak, V. R.; Hunt, M. R. C.; Šiller, L. Photoemission Spectroscopy of Clean and Potassium-Intercalated Carbon Onions. *Phys. Rev. B: Condens. Matter Mater. Phys.* **2003**, *67* (11), 113401.
(51) Butenko, Yu. V.; Chakraborty, A. K.; Peltekis, N.; Krishnamurthy, S.; Dhanak, V. R.; Hunt, M. R. C.; Šiller, L. Potassium Intercalation of Carbon Onions 'Opened' by Carbon Dioxide Treatment. *Carbon* **2008**, *46* (8), 1133−1140.
(52) Chacón-Torres, J. C.; Wirtz, L.; Pichler, T. Manifestation of Charged and Strained Graphene Layers in the Raman Response of Graphite Intercalation Compounds. *ACS Nano* **2013**, *7* (10), 9249−9259.
(53) Chacón-Torres, J. C.; Wirtz, L.; Pichler, T. Raman Spectroscopy of Graphite Intercalation Compounds: Charge Transfer, Strain, and Electron−Phonon Coupling in Graphene Layers. *Phys. Status Solidi B* **2014**, *251* (12), 2337−2355.
(54) Kim, J.; Kim, J.-R.; Lee, J.-O.; Park, J. W.; So, H. M.; Kim, N.; Kang, K.; Yoo, K.-H.; Kim, J.-J. Fano Resonance in Crossed Carbon Nanotubes. *Phys. Rev. Lett.* **2003**, *90* (16), 166403.
(55) Hasdeo, E. H.; Nugraha, A. R. T.; Sato, K.; Dresselhaus, M. S.; Saito, R. Electronic Raman Scattering and the Fano Resonance in

Metallic Carbon Nanotubes. *Phys. Rev. B: Condens. Matter Mater. Phys.* **2013**, *88* (11), 115107.
(56) Saitta, A. M.; Lazzeri, M.; Calandra, M.; Mauri, F. Giant Nonadiabatic Effects in Layer Metals: Raman Spectra of Intercalated Graphite Explained. *Phys. Rev. Lett.* **2008**, *100* (22), 226401.
(57) Onuma, H.; Kubota, K.; Muratsubaki, S.; Ota, W.; Shishkin, M.; Sato, H.; Yamashita, K.; Yasuno, S.; Komaba, S. Phase Evolution of Electrochemically Potassium Intercalated Graphite. *J. Mater. Chem. A* **2021**, *9* (18), 11187−11200.
(58) Billaud, D.; Henry, F. X. Structural Studies of the Stage III Lithium−Graphite Intercalation Compound. *Solid State Commun.* **2002**, *124* (8), 299−304.
(59) Bepete, G.; Hof, F.; Huang, K.; Kampioti, K.; Anglaret, E.; Drummond, C.; Pénicaud, A. Eau de Graphene" from a KC8 Graphite Intercalation Compound Prepared by a Simple Mixing of Graphite and Molten Potassium. *Phys. Status Solidi RRL* **2016**, *10* (12), 895−899.
(60) Share, K.; Cohn, A. P.; Carter, R. E.; Pint, C. L. Mechanism of Potassium Ion Intercalation Staging in Few Layered Graphene from in Situ Raman Spectroscopy. *Nanoscale* **2016**, *8* (36), 16435−16439.
(61) Trentino, A.; Madsen, J.; Mittelberger, A.; Mangler, C.; Susi, T.; Mustonen, K.; Kotakoski, J. Atomic-Level Structural Engineering of Graphene on a Mesoscopic Scale. *Nano Lett.* **2021**, *21* (12), 5179−5185.
(62) Frisch, M. J.; Trucks, G. W.; Schlegel, H. B.; Scuseria, G. E.; Robb, M. A.; Cheeseman, J. R.; Scalmani, G.; Barone, V.; Mennucci, B.; Petersson, G. A.; Nakatsuji, H.; Caricato, M.; Li, X.; Hratchian, H. P.; Izmaylov, A. F.; Bloino, J.; Zheng, G.; Sonnenberg, J. L.; Hada, M.; Ehara, M.; Toyota, K.; Fukuda, R.; Hasegawa, J.; Ishida, M.; Nakajima, T.; Honda, Y.; Kitao, O.; Nakai, H.; Vreven, T.; Montgomery, J. A., Jr.; Peralta, J. E.; Ogliaro, F.; Bearpark, M.; Heyd, J. J.; Brothers, E.; Kudin, K. N.; Staroverov, V. N.; Kobayashi, R.; Normand, J.; Raghavachari, K.; Rendell, A.; Burant, J. C.; Iyengar, S. S.; Tomasi, J.; Cossi, M.; Rega, N.; Millam, J. M.; Klene, M.; Knox, J. E.; Cross, J. B.; Bakken, V.; Adamo, C.; Jaramillo, J.; Gomperts, R.; Stratmann, R. E.; Yazyev, O.; Austin, A. J.; Cammi, R.; Pomelli, C.; Ochterski, J. W.; Martin, R. L.; Morokuma, K.; Zakrzewski, V. G.; Voth, G. A.; Salvador, P.; Dannenberg, J. J.; Dapprich, S.; Daniels, A. D.; Farkas, O.; Foresman, J. B.; Ortiz, J. V.; Cioslowski, J.; Fox, D. J. *Gaussian 09*, rev. D.01; Gaussian, Inc.: Wallingford, CT, 2009.
(63) Zeiger, M.; Jäckel, N.; Mochalin, V. N.; Presser, V. Review: Carbon Onions for Electrochemical Energy Storage. *J. Mater. Chem. A* **2016**, *4* (9), 3172−3196.
(64) Barnard, A. S. Modeling Polydispersive Ensembles of Diamond Nanoparticles. *Nanotechnology* **2013**, *24* (8), 085703.
(65) Melle-Franco, M.; Prato, M.; Zerbetto, F. Permanent Chiral Twisting of Nonchiral Carbon Nanotubes. *J. Phys. Chem. A* **2002**, *106* (19), 4795−4797.
(66) Bannwarth, C.; Ehlert, S.; Grimme, S. GFN2-XTB - An Accurate and Broadly Parametrized Self-Consistent Tight-Binding Quantum Chemical Method with Multipole Electrostatics and Density-Dependent Dispersion Contributions. *J. Chem. Theory Comput.* **2019**, *15* (3), 1652−1671.
(67) Cançado, L. G.; Jorio, A.; Ferreira, E. H. M.; Stavale, F.; Achete, C. A.; Capaz, R. B.; Moutinho, M. V. O.; Lombardo, A.; Kulmala, T. S.; Ferrari, A. C. Quantifying Defects in Graphene via Raman Spectroscopy at Different Excitation Energies. *Nano Lett.* **2011**, *11* (8), 3190−3196.
(68) Dresselhaus, M. S.; Jorio, A.; Saito, R. Characterizing Graphene, Graphite, and Carbon Nanotubes by Raman Spectroscopy. *Annu. Rev. Condens. Matter Phys.* **2010**, *1* (1), 89−108.
(69) Eckmann, A.; Felten, A.; Mishchenko, A.; Britnell, L.; Krupke, R.; Novoselov, K. S.; Casiraghi, C. Probing the Nature of Defects in Graphene by Raman Spectroscopy. *Nano Lett.* **2012**, *12* (8), 3925−3930.
(70) Lucherelli, M. A.; Raya, J.; Edelthalhammer, K. F.; Hauke, F.; Hirsch, A.; Abellán, G.; Bianco, A. A Straightforward Approach to Multifunctional Graphene. *Chem. - Eur. J.* **2019**, *25*, 13218−13223.

https://doi.org/10.1021/jacs.1c07604
J. Am. Chem. Soc. 2021, 143, 18997−19007